AGU PUBLICATIONS

JGR

Journal of Geophysical Research: Oceans

RESEARCH ARTICLE

10.1002/2015JC011491

Decadal-scale thermohaline variability in the Atlantic sector of the Southern Ocean

K. Hutchinson[1,2], S. Swart[1,3], A. Meijers[4], I. Ansorge[1], and S. Speich[5]

[1]Department of Oceanography, Marine Research Institute, University of Cape Town, Cape Town, South Africa, [2]South African Environmental Observations Network, SAEON Egagasini Node, Cape Town, South Africa, [3]Southern Ocean Carbon & Climate Observatory, CSIR, Rosebank, Cape Town, South Africa, [4]British Antarctic Survey, Cambridge, UK, [5]École Normale Supérieure, Department of Geosciences, Laboratoire de Météorologie Dynamique, Paris, France

Key Points:
- An adiabatic-diabatic Altimetry Gravest Empirical Mode is developed for the ACC south of Africa
- Anomalies separated in adiabatic and diabatic components exposing trends in frontal zones
- Antarctic Intermediate Water may be a sensitive indicator of climate change in the region

Correspondence to:
K. Hutchinson,
kath.hutchinson@gmail.com

Citation:
Hutchinson, K., S. Swart, A. Meijers, I. Ansorge, and S. Speich (2016), Decadal-scale thermohaline variability in the Atlantic sector of the Southern Ocean, *J. Geophys. Res. Oceans*, *121*, 3171–3189, doi:10.1002/2015JC011491.

Received 19 NOV 2015
Accepted 12 APR 2016
Accepted article online 19 APR 2016
Published online 14 MAY 2016

Abstract An enhanced Altimetry Gravest Empirical Mode (AGEM), including both adiabatic and diabatic trends, is developed for the Antarctic Circumpolar Current (ACC) south of Africa using updated hydrographic CTD sections, Argo data, and satellite altimetry. This AGEM has improved accuracy compared to traditional climatologies and other proxy methods. The AGEM for the Atlantic Southern Ocean offers an ideal technique to investigate the thermohaline variability over the past two decades in a key region for water mass exchanges and transformation. In order to assess and attribute changes in the hydrography of the region, we separate the changes into adiabatic and diabatic components. Integrated over the upper 2000 dbar of the ACC south of Africa, results show mean adiabatic changes of 0.16 ± 0.11°C decade^{-1} and 0.006 ± 0.014 decade^{-1}, and diabatic differences of -0.044 ± 0.13°C decade^{-1} and -0.01 ± 0.017 decade^{-1} for temperature and salinity, respectively. The trends of the resultant AGEM, that include both adiabatic and diabatic variability (termed AD-AGEM), show a significant increase in the heat content of the upper 2000 dbar of the ACC with a mean warming of 0.12 ± 0.087°C decade^{-1}. This study focuses on the Antarctic Intermediate Water (AAIW) mass where negative diabatic trends dominate positive adiabatic differences in the Subantarctic Zone (SAZ), with results indicating a cooling (-0.17°C decade^{-1}) and freshening (-0.032 decade^{-1}) of AAIW in this area, whereas south of the SAZ positive adiabatic and diabatic trends together create a cumulative warming (0.31°C decade^{-1}) and salinification (0.014 decade^{-1}) of AAIW.

1. Introduction

The Southern Ocean plays a critical role in the global circulation, as it links the three major ocean basins, and connects the deep sea to the surface [*Marshall and Speer*, 2012]. The principal flow of the Southern Ocean, the Antarctic Circumpolar Current (ACC), extends uninterrupted around Antarctica and is associated with steeply sloping isopycnals maintained by the intense westerlies and strong meridional density gradients [*Killworth and Hughes*, 2002]. The ACC exerts a critical influence on water mass formation, subduction, and in turn climate regulation, via the redistribution of heat, salt, and atmospheric gasses [*Böning et al*., 2008]. In recent decades, this vital limb of the global ocean conveyor belt has been in a state of disequilibrium with the atmosphere and cryosphere, with hydrographic station and Argo float observations revealing rising temperatures and freshening trends in the upper 1000 m [*Jacobs*, 2006; *Aoki et al*., 2005; *Böning et al*., 2008].

In the Atlantic sector of the Southern Ocean, waters from the Indian, South Atlantic, and Southern Oceans meet and interact through highly energetic, nonlinear dynamics that lead to intense water mass mixing and transformation [*Lutjeharms*, 1996; *Swart and Speich*, 2010; *Rusciano et al*., 2012; *Rimaud et al*., 2012]. Furthermore, the interoceanic exchange of water that ensues, and the meridional heat transport in the South Atlantic, are considered critical factors in determining global climate [*Fu*, 1981; *Holfort and Siedler*, 2001; *Garzoli and Matano*, 2011]. Despite the importance of this region, changes in thermohaline properties and water mass evolution are relatively poorly understood due to the scarcity of high-resolution and extended time series data, as well as the difficulties that exist when attempting to model such a dynamic system [*Meredith and Hogg*, 2006; *Speich et al*., 2006; *Rimaud et al*., 2012].

The traditional observational methodology of the ACC density field has been via the acquisition of in situ temperature and salinity profiles. However, the resource intensive nature of obtaining these data means that it is highly challenging to monitor the current with sufficient resolution to avoid aliasing, as the uneven

spatial and temporal distribution of data is the largest source of uncertainty in reporting Southern Ocean thermohaline property modification [*Sokolov et al*., 2004; *Jacobs*, 2006; *Gille*, 2008]. An effective approach to address this is to develop a proxy technique based on a variable that can be measured at a higher spatial and temporal resolution requiring fewer resources [*Watts et al*., 2001; *Sokolov et al*., 2004]. *Sun and Watts* [2001] first demonstrated that there is a highly robust empirical relationship between the surface dynamic height of the water column and the subsurface temperature and salinity profiles within the Southern Ocean. This form of proxy methodology is termed the Gravest Empirical Mode (GEM), and is highly effective in the Southern Ocean due to the steep meridional density gradients and the equivalent barotropic nature of the ACC [*Killworth*, 1992]. This means that subsurface changes in density are highly correlated with variability in surface expressions, such as dynamic height or sea surface height [*Vivier et al*., 2005; *Firing et al*., 2011].

A GEM proxy technique based on that developed originally by *Meinen and Watts* [2000] is used here to establish the relationships between the thermohaline properties of the upper 2000 dbar of the water column and the surface dynamic height [*Watts et al*., 2001; *Sokolov et al*., 2004]. The main improvements of this GEM compared to past studies are the use of Argo profiling float data in addition to more recent repeat CTD hydrography data as well as a more appropriate technique for the removal of the seasonal bias. Satellite measurements of sea surface height anomalies are available for the region of the ACC south of Africa from 1992, and therefore by coupling the GEM dynamic height relationship with altimetry measurements, an enhanced altimetry-based GEM (AGEM) is produced following the methods of *Swart et al*. [2010] and *Meijers et al*. [2011b]. From this AGEM, 20 years of weekly temperature and salinity sections for the region from 1992 to 2012 can be analyzed.

The AGEM generated fields are utilized to observe the temporal evolution of Antarctic Intermediate Water (AAIW) in the south-east Atlantic sector of the Southern Ocean. This water mass was chosen as it feeds the base of the thermocline in the Southern Hemisphere oceans, thereby acting as an important limb of the global Meridional Overturning Circulation (MOC), and providing a teleconnection between future ocean changes and past and present variations in the Southern Ocean. This water mass facilitates important transports of heat, freshwater, and biogeochemical tracers both vertically from the surface to the interior ocean, and meridionally from the Southern Ocean to the tropics [*Sloyan and Rintoul*, 2001; *Pahnke et al*., 2008]. The water mass undergoes significant modification of its properties as it experiences high levels of mixing crossing from the South Atlantic to the South Indian Ocean [*Rimaud et al*., 2012]. From Argo float data, *Rusciano et al*. [2012] identified the exact isopycnal interval of AAIW as being 27.1–27.32 kg m^{-3} at the GoodHope (GH) line (approximate longitude range 0°E–10°E). It therefore accepted that in the southeast Atlantic, all varieties of intermediate water are found to reside between 27.0 and 27.4 kg m^{-3}, and eastward of this area, the water mass becomes saltier and resides deeper [*Rusciano et al*., 2012]. Circumpolar warming has been detected within the AAIW layer [*Schmidtko and Johnson*, 2012]; however, due to the scarcity of high-resolution data for the southeast Atlantic, the extent of water mass change in this area is poorly understood [*Banks et al*., 2000; *Pahnke et al*., 2008]. The contribution of the Atlantic sector of the Southern Ocean to regulating climate, coupled with the influence of AAIW on the stability of the ocean circulation system, makes obtaining a better view of the extent of property evolution in this area of significant importance.

The study presents how the existing GEM methodology is enhanced by including more recent, higher spatial and temporal resolution in situ Southern Ocean data that include both CTD and Argo float measurements. The GEM and AGEM techniques along with the hydrography used to set up these proxy relationships allow for the explicit separation of the diabatic and adiabatic components of change in a regional study. The adiabatic trends are calculated from a linear regression and correlation of the AGEM generated thermohaline fields. The diabatic trends on the other hand are obtained through the investigation of the changes evident in the in situ hydrographic data. Previous studies [e.g., *Böning et al*., 2008; *Meijers et al*., 2011b] addressed global changes and therefore smoothed much of the regional variability in creating a circumpolar average of the results. The strength of this study lies in the focused analysis that provides improved insight into a certain sector of the Southern Ocean.

2. Data

2.1. CTD Data

The GoodHope (GH) line is a repeat monitoring track that spans the ocean between Africa and Antarctica [*Speich and Arhan*, 2007; *Speich and Dehairs*, 2008; *Swart et al*., 2008]. A total of 11 CTD sections occupying, or in close

Table 1. Summary of the CTD Sections Used in This Study

Section	Date	Institute	Ship	Chief Scientist/Reference
AJAX	Jan 1984	*Scripps Institution of Oceanography*	R/V Knorr	Reid/*Whitworth and Peterson* [1985]
A21	Jan–Mar 1990	*University of Hamburg*	R/V Meteor	W. Roether/*Roether et al.* [1990]
A12	May–Aug 1992	*Leibniz-Institut für Meereswissenschaften, Kiel* (LfMK)	R/V Polarstern	P. Lemke/*Lemke* [1992]
A1299	Mar 1999	*Alfred Wegener Institute*	R/V Polarstern	E. Fahrbach
A1200	Dec 2000	*Alfred Wegener Institute*	R/V Polarstern	E. Fahrbach/*World Ocean Circulation Experiment* [2002]
A1202	Dec 2002	*Alfred Wegener Institute*	R/V Polarstern	Fütterer/*World Ocean Circulation Experiment* [2002]
GH2004	Nov 2004	*Shirshov Institute of Oceanology*	RV Akademik Sergey Vavilov	S. Gladyshev/*Gladyshev et al.* [2008]
GH2005	Oct 2005	*Shirshov Institute of Oceanology*	RV Akademik Sergey Vavilov	S. Gladyshev/*Gladyshev et al.* [2008]
GH2006	Oct–Nov 2006	*Shirshov Institute of Oceanology*	RV Akademik Sergey Vavilov	S. Gladyshev/*Gladyshev et al.* [2008]
BGH2008	Mar–Apr 2008	*Laboratoire de Physique des Oceans*	RV Marion Dufresne II	S. Speich/*Speich and Dehairs* [2008]
GH2009	Dec 2009	*Shirshov Institute of Oceanology*	RV Akademik Sergey Vavilov	S. Gladyshev

proximity to, the GH line have been selected for this GEM study (all stations reach a maximum depth of at least 2000 dbar; information available in Table 1; station positions shown in Figure 1). These sections span the period from 1984 to 2009, with five transects occupied during the World Ocean Circulation Experiment (WOCE; completed in the late 1990s), and the remainder occupied during GH transects undertaken between 2004 and 2009. In total, 556 CTD stations covering the region 38°S to 56°S have been used in this study. The 2000 dbar maximum depth was used as this corresponded to the limit of Argo data available. For further information regarding CTD calibration and sampling techniques, refer to the references provided in Table 1.

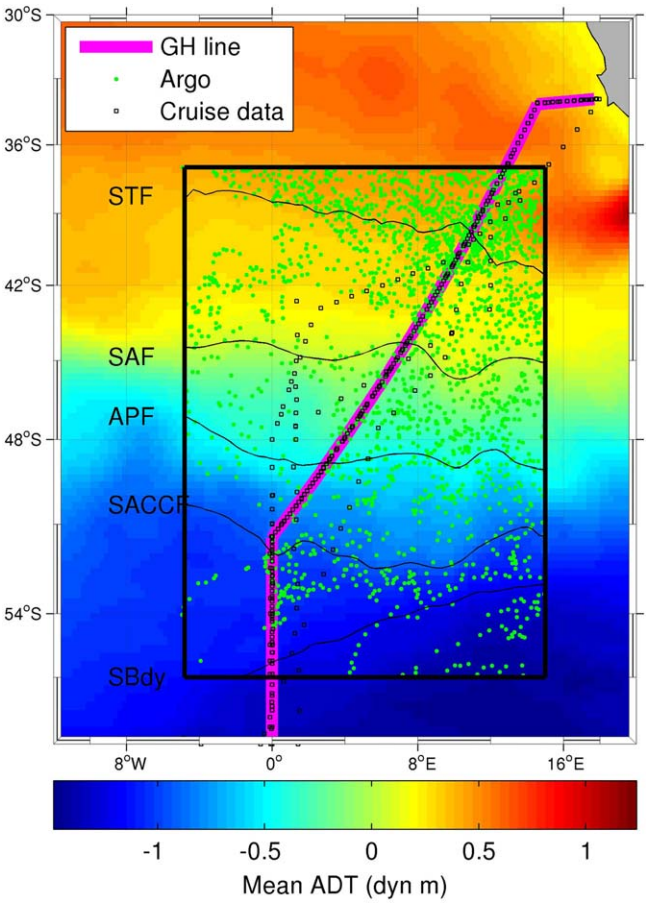

Figure 1. Mean Absolute Dynamic Topography (ADT) [*Rio et al.*, 2009] for the region (in dyn m) from 1992 to 2012, with the positions of the hydrographic stations used in this study overlaid. The position of the GH line is marked with a magenta line. The limits of the study region and float data used are delineated with the black box. Average positions of the ACC fronts as defined from altimetry, using the regional dynamic height signatures identified by *Swart et al.* [2010] are overlaid.

2.2. Argo Float Data

The Argo float program has proven to be invaluable in collecting data in remote regions such as the Southern Ocean [*Riser et al.*, 2016; *Roemmich et al.*, 2015, 2003; *Gould et al.*, 2004]. In this study, a total of 155 floats, sampling between 2004 and 2012, were found to be located in the study domain (37°S–56°S; 5°W–15°E) surrounding the GH line (Figure 1). The domain limits of the study were selected to balance the benefits of including a wider data set from which to build the GEM relationships, with the negative impact of incorporating measurements of significantly different water masses. The 155 floats located within the domain rendered an additional 2201 profiles used to set up the GEM fields. The data are delayed mode and underwent quality control, with further quality checks performed by the CLIVAR international observing program.

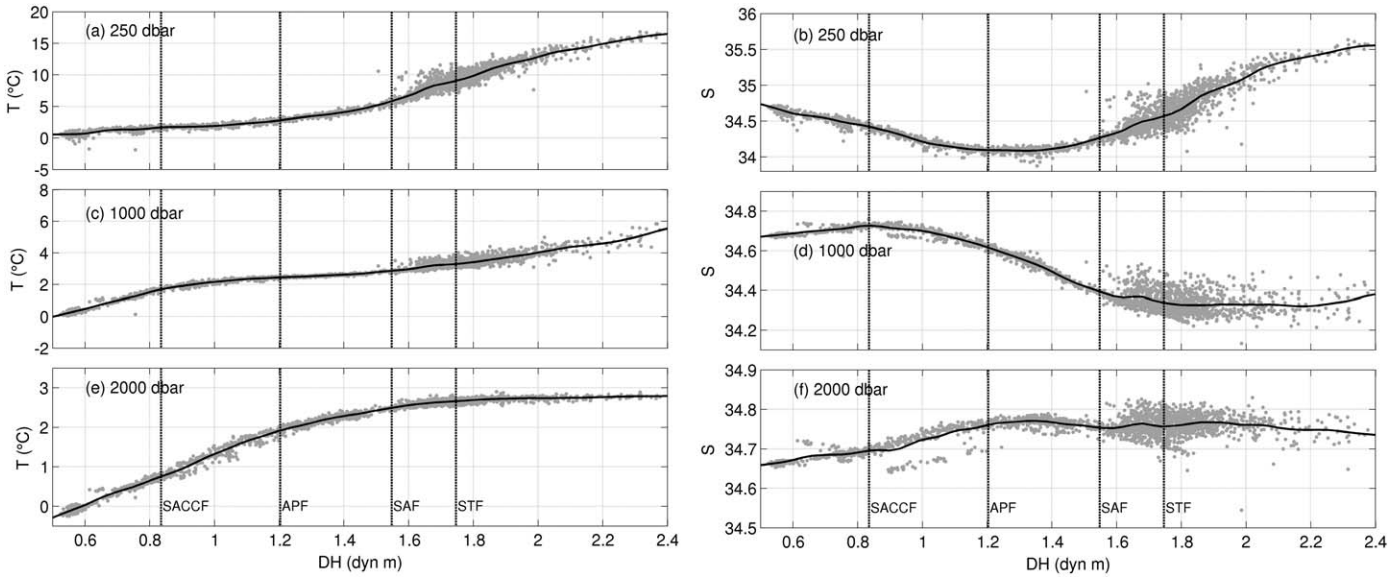

Figure 2. (a, c, e) Temperature and (b, d, f) salinty data obtained from all available cruise and Argo float data plotted against dynamic height (DH; φ) for three different pressure levels. The data are fitted with a smoothing spline. The mean positions of the Southern Ocean fronts are indicated. The location of the Subtropical Front (STF) represents the northern boundary of the GEM. The Subantarctic Front (SAF) separates the tightly fit ACC data from the turbulent Cape Cauldron and the associated Agulhas Ring shedding region to the north.

2.3. Satellite Altimetry

The satellite measurements used in this study are AVISO updated delayed weekly maps of sea level anomalies (MSLA), gridded onto a 1/3° spatial resolution, and date from October 1992 to February 2012. For details on the mapping methods and error corrections applied to these fields, refer to *Le Traon et al*. [1998], *Le Traon and Ogor* [1998], and *Ducet et al*. [2000]. These maps provide circumpolar sea level anomalies (SLA), and therefore an interpolation onto the GH line coordinates was required. A mean dynamic topography (MDT) was then added to the satellite product to obtain an absolute dynamic topography (ADT) for the region. In this study, the MDT was calculated from a synthesis of all available relevant hydrographic data and referenced to 2000 dbar, as this was found to more accurately represent the region compared to the AVISO MDT product [*Rio et al*., 2009], and the reference level is compatible with the hydrographic dynamic heights used in the GEM. The ADT is then calculated as the sum of the MDT from hydrography plus the AVISO SLA measurements. In total, 1009 weeks of MSLA combined with the MDT were utilized to generate a time series of the thermohaline fields covering 20 years. Please note that the frontal locations were identified using the dynamic height signatures from *Swart et al*. [2010] located on the *Rio et al*. [2009] maps of dynamic topography. The latitudinal positions of the fronts on the GH line at each time step were obtained and the corresponding ADT noted (SLA plus local calculated MDT). It is for this reason that the dynamic height values of Figure 1 differ to the dynamic heights in Figure 2, as Figure 2 is the ADT calculated specifically for the GH line and referenced to 2000 dbar.

3. An Enhanced GEM for the South Atlantic

The GEM method, described first by *Sun and Watts* [2001], utilizes all historical casts by projecting the data into baroclinic stream function space. The GEM field contains information from all available historical hydrographic data and therefore provides an improved resolution than individual transect [*Sun and Watts*, 2002]. *Swart et al*. [2010] were the first to establish a GEM for the southeast Atlantic sector of the Southern Ocean based on data from seven CTD transects of the ACC, and relate the GEM to satellite altimetry. A drawback of this study was the limited data upon which the proxy relationship was built. The research presented here, on the other hand, utilizes updated cruise data (11 CTD transects) along with a vast inventory of Argo profiling float measurements, to develop GEM proxy relationships based on a far greater array of reference points. The CTD data for the Southern Ocean are largely seasonally biased as most cruises are restricted to

the austral spring-summer months. Prior to synthesizing all data to establish the GEM relationships, measurements pertaining to the top 300 dbar required "deseasoning." This was achieved by binning the data into frontal zones and removing the seasonal influence defined from Argo data using a 3 month low-pass filter of monthly anomalies from the annual mean. This removed contributions to dynamic height due to seasonal variability in the upper ocean that otherwise would have been erroneously attributed to the adiabatic movement of the entire water column.

The hydrographic data are projected into streamline space parameterized by pressure (p) and dynamic height (φ). To do so, the surface φ, relative to 2000 dbar, was obtained for every hydrographic profile and plotted against the temperature (T) and salinity (S) values for that profile at each pressure level between the surface and 2000 dbar, at 5 dbar intervals (Figure 2). The scatter of the relationships (Figure 2) displays remarkable organization around a functional curve. A cubic smoothing spline provides an effective approximation method [*Thomson and Emery*, 2014] that can be fitted to the scatter (coefficient of 0.9997 is used). This spline coefficient was chosen after extensive testing as the best fit for the results as it captures the hydrographic variability in the region without possessing too much sensitivity to outliers.

It is evident from Figure 2 that the scatter about the smoothing spline increases with higher φ and that the magnitudes of scatter about the splines increase with decreasing depth (e.g., 250 dbar) and at φ greater than 1.6 dyn m (extending northward of the Subantarctic Zone, SAZ). The phenomena driving these deviations are related to the presence of mesoscale and submesoscale features, such as eddies associated with the Agulhas Retroflection, and Subtropical Front (STF) instabilities that prevail in this region [*Swart and Speich*, 2010; *Dencausse et al*., 2010]. The coexistence of varying φ over time in one location is synonymous with this highly variable area associated with the Agulhas Current system and its leakage into the South Atlantic Ocean [*Boebel et al*., 2003; *Swart and Speich*, 2010; *Rusciano et al*., 2012]. The presence of multiple T(φ,p) and S(φ,p) profiles along one streamline presents a challenge for the GEM, which assumes a single mode, and thus we limit the generated fields of the ACC to south of 38°S (or $\varphi \sim$1.75 dyn m), which is the approximate latitude of the geographical STF. This allows for the inclusion of the SAZ in the resultant fields and part of the overall ACC analysis (see section 3.3 where the GEM-related errors are discussed in detail).

4. Altimetry-Based GEM and Testing

An Altimetry GEM (AGEM) is created for the region of the ACC south of Africa by combining the established GEM relationships with an altimetry-derived ADT product (see section 2.3), as previously done by *Swart et al*. [2010]. The GEM produces T(φ,p) and S(φ,p) fields where φ is dynamic height (see Figure 2 for illustration of process). By drawing on an approximate 1:1 equivalence between the satellite ADT η(x,y,t) and φ from the GEM fields, the AGEM is then able to generate T(x,y,p,t) and S(x,y,p,t) fields relevant for the GH line at weekly time steps from October 1992 to February 2012 ($\sim$20 years). The time mean satellite η(x,y) field can be seen in Figure 1. The suitability of the GEM technique in the Southern Ocean has been demonstrated by a number of studies [*Meinen and Watts*, 2000; *Watts et al*., 2001; *Sokolov et al*., 2004; *Swart et al*., 2010; *Meijers et al*., 2011a]. We have therefore only presented here the comparisons with the in situ cruise observations pertaining to the final AGEM. For the sake of brevity, we present and discuss the comparison between the GEM and three CTD transects, namely GH2004, GH2008, and GH2009. These CTD occupations are considered the most appropriate for comparison as they show the range of proficiency of the AGEM, from the most inaccurate reproduction (GH2004) to the most accurate (GH2009). Note that the CTD data against which the AGEM are compared is removed from the synthesis of hydrographic profiles that are projected into stream function space to ensure the independence of the test data.

Figure 3 shows the differences between the AGEM T(x,y,p) and salinity S(x,y,p) sections corresponding to the sampling dates of each cruise and the original CTD observations (AGEM-CTD). Overall, the AGEM is capable of capturing the thermohaline structure for all three cruises. Elevated differences are visible in the upper 1000 dbar of the northern section of all transects. These larger offsets (also identified in Figure 2) are an artifact of the GEM process, whereby the T and S profiles of an entire column are laterally shifted to the location of the corresponding φ, translating to an "adiabatic" alteration. The AGEM therefore misinterprets a change in φ as a shift in water masses, whereas it may instead be due to diabatic fluctuations in heat or salt flux, barotropic variability, or baroclinic variability below 2000 dbar. The T and S differences decrease significantly south of $\sim$42°S and at pressures greater than 500 dbar (Figure 3). Note that for all comparisons, the

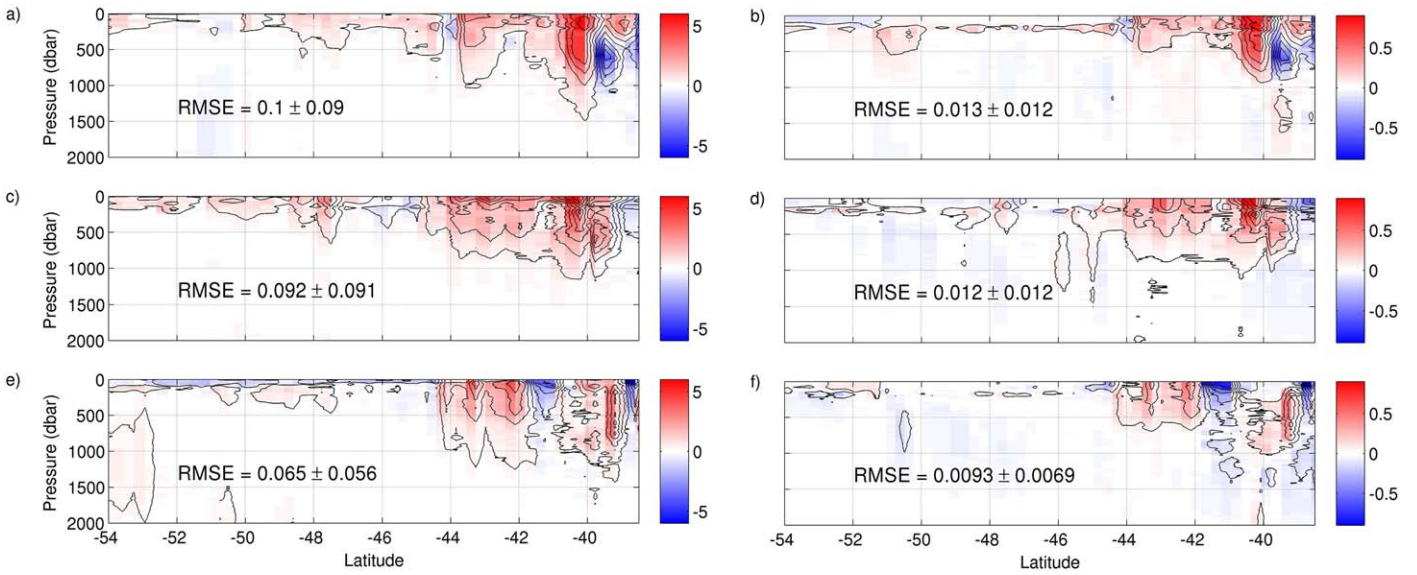

Figure 3. Temperature difference between AGEM and original cruise measurements at all latitudes (AGEM-CTD) for (a) GH2004, (c) GH2006, and (e) GH2009 tests. Salinity difference between AGEM and original cruise values for (b) GH2004, (d) GH2006, and (f) GH2009 tests. The root-mean-square error (RMSE) of the residuals in the upper 2000 dbar, and the standard deviation thereof, are reported for each comparison.

AGEM appears to underestimate salinity in the interior of the ACC (negative differences, Figures 3b, 3d, and 3f). Overall, the RMS errors from the cruise comparisons were found to show good agreement of the AGEM fields with observations. The offsets are largest for the GH2004 comparison, with the RMS errors decreasing with each consecutive cruise—GH2006 and GH2009. The connection between AGEM accuracy increasing with progressive cruise dates may be a result of regular improvements in the satellite altimetry data quality providing a more accurate SLA and thus ADT [*Le Traon et al*., 1998]. The percentage of observed variance represented by the AGEM fields varies per cruise with 84.4%, 90.7%, and 92.4% of the T variability and 74.4%, 81.7%, and 78.4% of the S fluctuations captured for the GH2004, GH2006, and GH2009 comparisons, respectively. The amount of variance captured by the AGEM presented here is lower than that reported by *Sun and Watts* [2001] and *Swart et al*. [2010] as this AGEM extends further north to 38°S versus the 45°S limit of the variance test at the WOCE SR3 line of *Sun and Watts* [2001] and 40°S by *Swart et al*. [2010]. The AGEM therefore struggles to accurately represent all the water mass properties present at the northern limits of the domain.

The average RMS error of the T residuals were 0.22 ± 0.056°C, 0.15 ± 0.071°C, and 0.086 ± 0.082°C for the upper 300, 1000, and 2000 dbar, respectively. The average RMS reported by *Swart et al*. [2010] for the top 2500 of their AGEM was 0.15°C. The RMS T residuals of the satGEM developed by *Meijers et al*. [2011a] also decreased rapidly below the thermocline with a surface RMS value of 1.16°C, decreasing to a RMS error of 0.45°C at 500 dbar and 0.11°C at 1500 dbar. The RMS errors shown here are in general smaller than those reported by both *Swart et al*. [2010] and the circumpolar satGEM developed by *Meijers et al*. [2011a]. This AGEM is also shown to be more accurate than the second version of the 2013 World Ocean Atlas [*Locarnini et al*., 2013], which exhibits standard errors in T of approximately 0.5°C in the top 300 m and 0.3°C at 1000 m depth.

The salinity RMS errors of the AGEM are similarly acceptable, with the mean RMS offset over all comparisons being 0.031 ± 0.0078, 0.019 ± 0.0108, and 0.012 ± 0.011 for the upper 300, 1000, and 2000 dbar, respectively. *Swart et al*. [2010] reported mean S offsets of 0.02 for the upper 2500 dbar, and the satGEM of *Meijers et al*. [2011a] possessed an RMS error of 0.132 at the surface, decreasing to less than 0.03 below 1000 dbar. The RMS errors calculated for the AGEM are comparable in magnitude to the standard S errors of World Ocean Atlas 2013, which are in the order of 0.02–0.05 at 500 m depth, in the region south of Africa [*Zweng et al*., 2013]. The reduction in error in this improved version of the AGEM is likely due to the inclusion of Argo data providing more spatially and temporally coherent GEM fields from which to derive the thermohaline sections using altimetry.

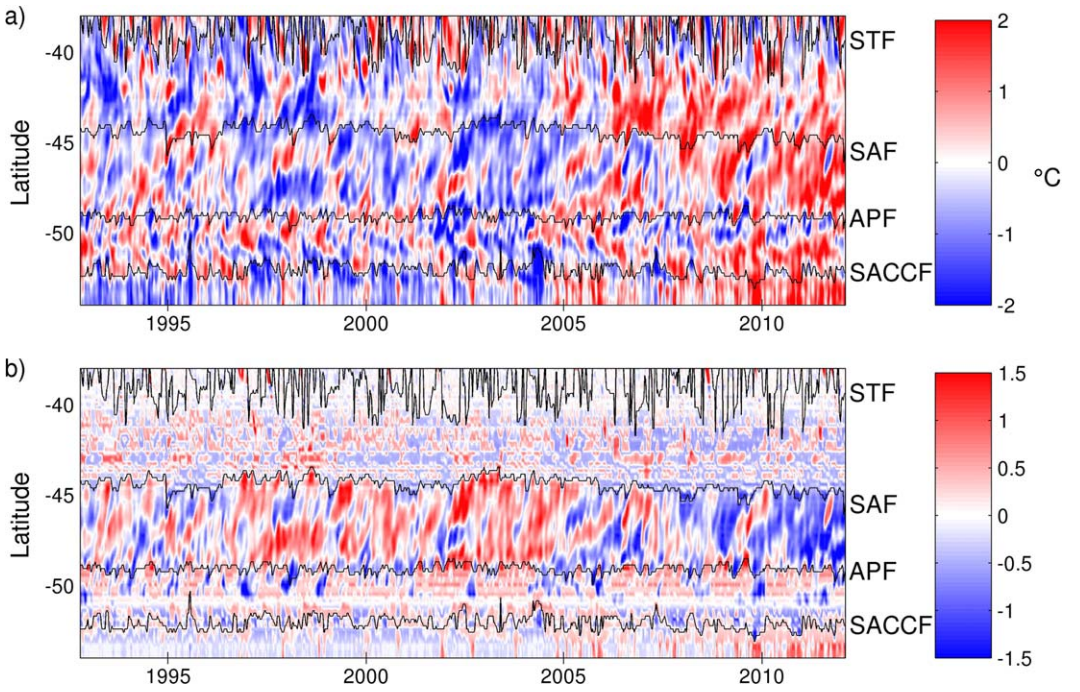

Figure 4. Hovmöller representation of (a) temperature and (b) salinity anomalies, normalized by the local standard deviation at each depth and averaged over the upper 2000 dbar from a 20 year AGEM time series along the GoodHope line south of Africa. The positions of the main ACC fronts as defined by *Swart et al*. [2010] are shown in black and labeled.

5. Results

5.1. Adiabatic and Diabatic Trends

The GEM and AGEM projections along with the hydrography used to create these proxies enable the separation of the observed changes into the adiabatic and diabatic components. We assume stationarity in our data, even though we are aware that this is incorrect. We have 20 years of variability in the AGEM time series and so the lowest frequency we can resolve is 10 years. The results presented here discuss this decadal low frequency, and are referred to as "trends," which denote the amplitude of low-frequency variability (which is admittedly underrepresented as it is poorly resolved). We describe the amplitude of this frequency using a linear regression as the assumption that the variability is linear provides for clearer interpretation and evaluation.

The success of the AGEM technique at reproducing observations in the African sector of the Southern Ocean is largely due to the equivalent barotropic nature of variability (adiabatic shifting), and the proficiency of the GEM upon which the AGEM is built. For the region and scales relevant to this study, adiabatic shifts from frontal movements and mesoscale activity largely determine sea surface height variability. We therefore assume that columns of water largely retain their vertical structure during horizontal displacements [*Watts et al*., 2001]. The adiabatic differences $Ta'(\varphi,p)$ and $Sa'(\varphi,p)$ can thus be obtained using the time evolving AGEM fields as is explained in section 5.1.1 following the method of *Meijers et al*. [2011b]. These trends (Figure 5) represent the horizontal displacement of water masses, which in the ACC represents a shift in the position of the circumpolar fronts. Diabatic adjustments, on the other hand, do not necessarily conserve dynamic height and signify a change in water mass properties due to heat and freshwater fluxes or mixing. The residuals between two GEMs created from the historical in situ hydrographic profiles with different temporal means denote the changing thermohaline structure due to alterations that are independent of frontal shifts [*Meijers et al*., 2011b]. The method to find diabatic $Td'(\varphi,p)$ and diabatic $Sd'(\varphi,p)$ is clearly explained in section 5.1.2. It is important to understand both the adiabatic and diabatic components of change if we are to understand the main drivers of thermohaline variations in the ACC.

5.1.1. AGEM Variability—Adiabatic Trends Due to a Shift in Circumpolar Fronts

The AGEM generated 20 years of weekly T(x,y,p) and S(x,y,p) sections of the upper 2000 dbar, meridionally across the ACC south of Africa, at the GH line. The thermohaline profiles have a spatial resolution of 1/3° latitude,

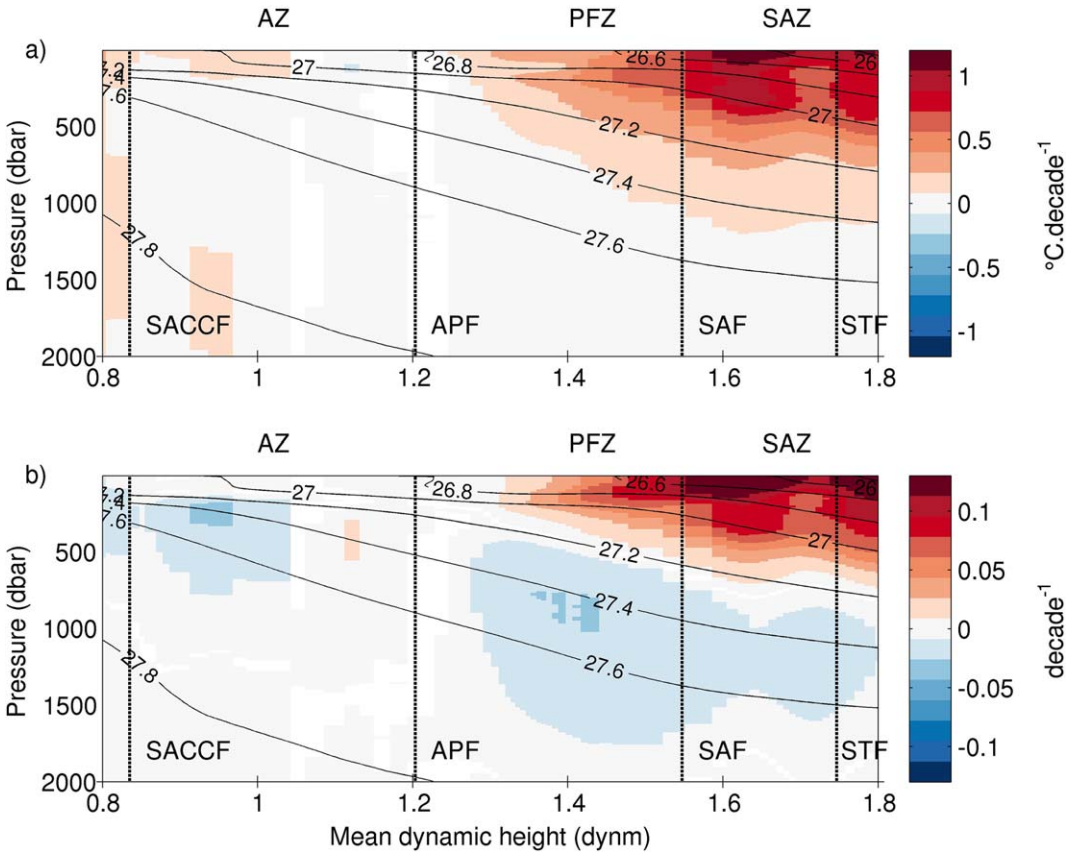

Figure 5. Adiabatic trends per decade for (a) temperature (°C decade^{-1}) and (b) salinity (decade^{-1}). Only the trends with a correlation coefficient significant greater than 95% confidence are plotted. Potential density contours and the mean positions of the ACC fronts have been overlaid.

matching the sampling resolution of the satellite SLA data. A Hovmöller representation (Figure 4) provides insight into the vertical integral over the top 2000 dbar of T(x,y,t) and S(x,y,t) variability over 20 years showing the normalized anomalies from the mean property values at constant latitudes. The anomaly from the 20 year mean at each depth is divided by the standard deviation of all anomalies over time at this depth, and then all normalized anomalies are averaged over the upper 2000 dbar. In doing this, the influence of highly variable areas is reduced and the relative influence of large anomalies in areas with small variability is highlighted. Positive T anomalies (with normalized values up to 3°C) are located between the STF and Subantarctic Front (SAF) post-2005. The normalized S anomalies in the SAZ are small as there is a high level of local variability (influence of Agulhas Rings and STF instabilities) thereby further highlighting the significance of the large normalized T values. Post-2007, positive T anomalies are observed over the entire meridional extent of the ACC, with strongly negative S anomalies (values up to 1.5) in the Polar Frontal Zone (PFZ) (Figure 4b).

The adiabatic Ta′ (x,y,p) and Sa′ (x,y,p) changes are obtained from the time evolving AGEM fields by estimating the linear temporal trend in each property at each grid point. These trends can then be projected back into φ space using the MDT at that location (calculated from the hydrographic data and referenced to 2000 dbar) plus the satellite SLA at each altimetry time step. The resultant adiabatic Ta′(φ,p) and adiabatic Sa′(φ,p) changes per decade are shown in Figure 5. The results are presented in φ space due to the circumpolar variations in the meridional position of the ACC, thereby allowing for comparison with other sectors of the Southern Ocean. At each grid point (p, φ), the linear regression and correlation coefficients are calculated for the T and S data with time. Only the correlations with significance greater than 95% confidence were plotted and the gradient of the linear regression fit reported.

The adiabatic trends presented here are similar in pattern to the circumpolar mean adiabatic T and S trends of *Meijers et al.* [2011b], however, the trends are over double the magnitude of those reported by *Meijers*

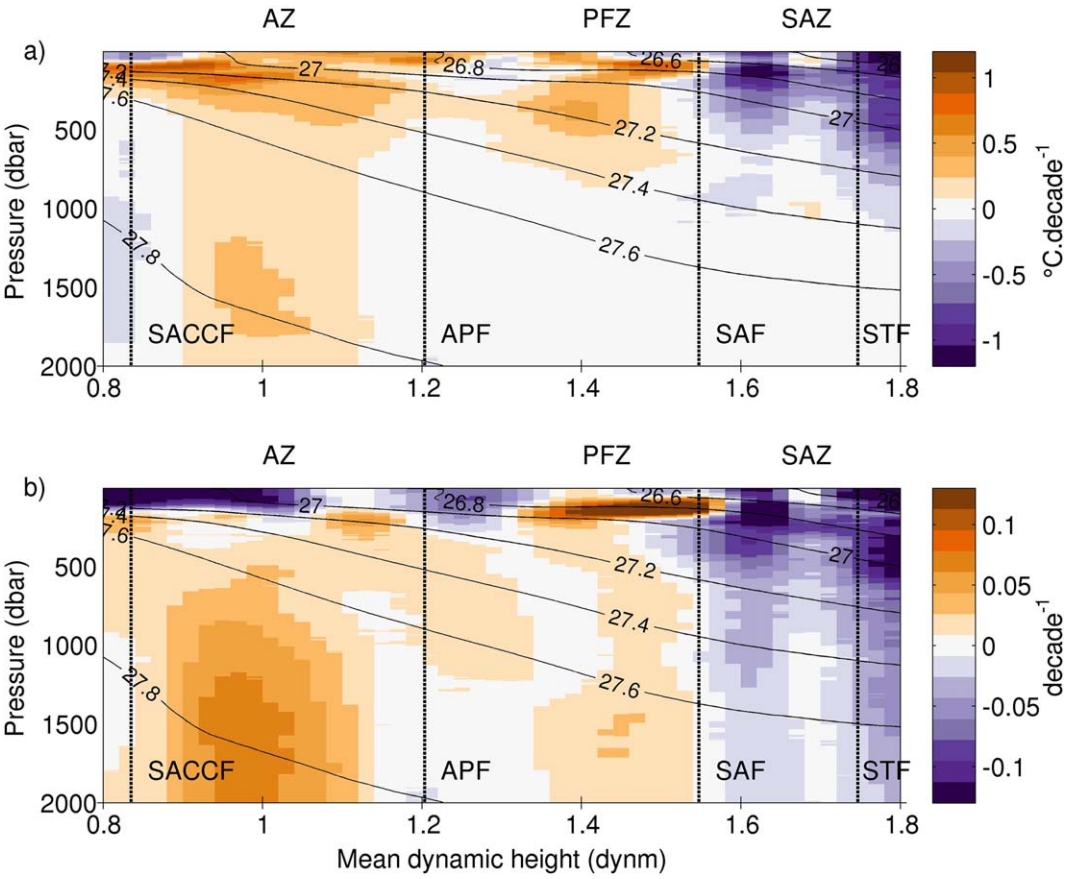

Figure 6. Diabatic differences per year between GEMs with temporal means of 2000 and 2007 for (a) temperature (°C decade^{-1}) and (b) salinity (decade^{-1}). Potential density contours and the mean positions of the ACC fronts in dynamic height space have been overlaid.

et al. [2011b] who reported maximum T and S trends of approximately ~0.04°C yr^{-1} and 0.005 yr^{-1}. We estimate maximum yearly trends of 0.12°C yr^{-1} and 0.013 yr^{-1} for the adiabatic changes reported here (or 1.2°C decade^{-1} and 0.13 decade^{-1}, Figures 5a and 5b). The focus of this study is on the point that the changes are regionally specific, therefore highlighting the local anomalies that are likely removed by circumpolar averaging in *Meijers et al*. [2011b]. The mean adiabatic change in T and S for the upper 2000 dbar of the ACC south of Africa is 0.16 ± 0.11°C decade^{-1} and 0.006 ± 0.014 decade^{-1}. Between the 26.6 and 27.2 kg m^{-3} contours, an overall persistence of positive anomalies is visible in Figure 5, with a warming of 0.6°C decade^{-1} and salinification of 0.07 decade^{-1}. A layer of freshening is located below the 27.2 kg m^{-3} isopycnal, belonging to UCDW with decreases in S of −0.06 decade^{-1}. A net warming and increase in salinity between the surface and intermediate depths was also reported by *Meijers et al*. [2011b], with weak adiabatic freshening below AAIW and a similar maximum in negative trends observed just south of the SAF (see Figure 5b at 1000 dbar, 1.4 dyn m).

5.1.2. Diabatic Trends Due to Heat and Freshwater Fluxes

The diabatic Td′(φ,p) and Sd′(φ,p) variability not associated with frontal movement is calculated using the historical hydrographic observations. By observing the trend from in situ observations with time, the temporal shift in thermohaline properties can be extracted. As these changes are separate from the coherent equivalent barotropic adiabatic moment of water masses discussed in the previous section, and may be produced by surface property fluxes or lateral mixing, we term these trends diabatic. Two GEMs with different temporal means are established from the in situ CTD and Argo measurements, and the difference between the two is used to calculate the diabatic trends in the region over the sampling period. The year 2005 was used to divide the hydrographic data used to create the separate GEMs because this year allows for an even data distribution, and is still approximately mid-time series. The pre-2005 GEM had a mean date of 22 September 2000 and the post-2005 had a mean date of 21 October 2007, with a resultant time offset

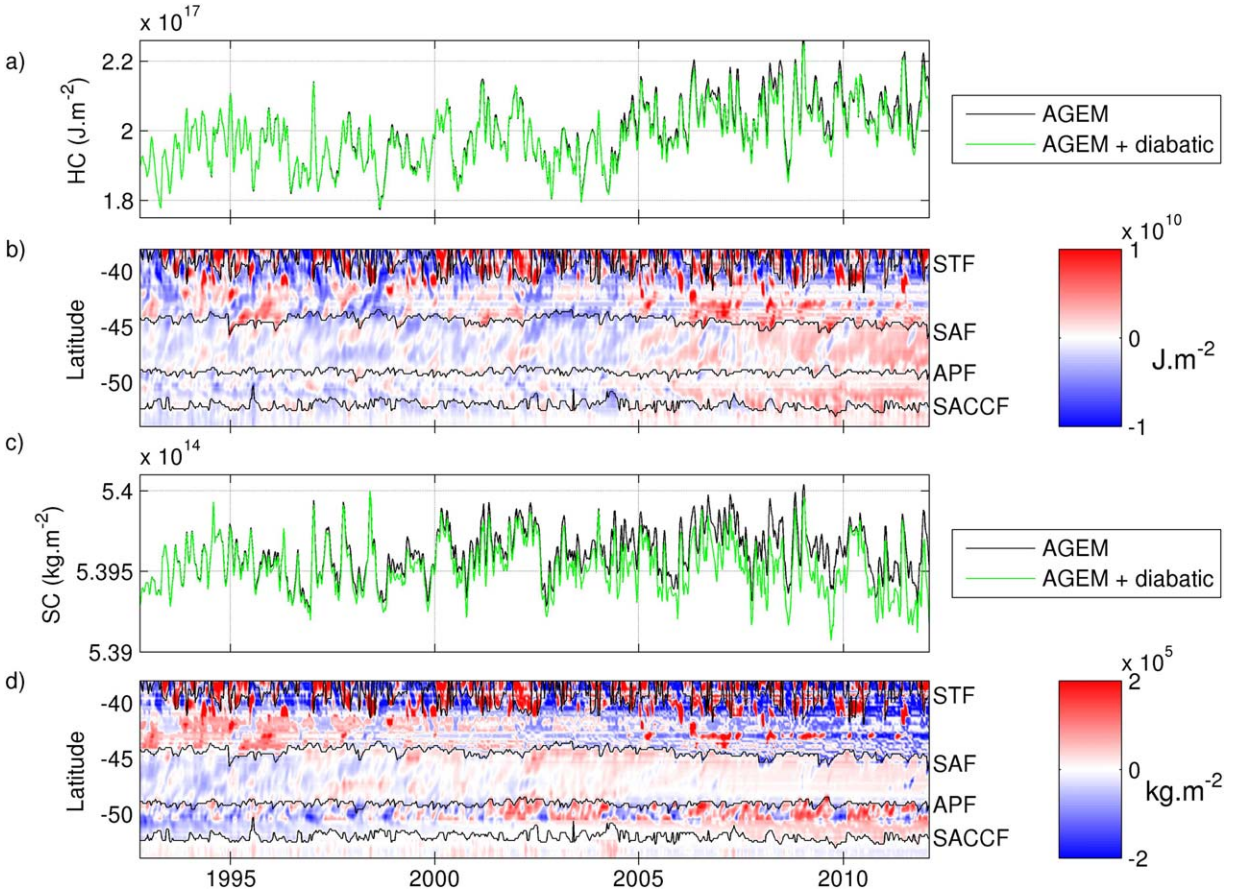

Figure 7. Comparison between original and AD-AGEM estimates of (a) heat and (c) salt content integrated over the upper 2000 dbar, across the ACC south of Africa. Hovmöller plots showing the evolution of ACC (b) heat and (d) salt content anomalies with latitude and time calculated from the AD-AGEM fields. The latitude of the ACC fronts, as determined with satellite altimetry data, are overlaid in Figures 7b and 7d.

in the GEM fields of 7.08 years. The differences between two the GEMs at each grid point were converted into trends per decade Td′(φ,p) and Sd′(φ,p) and essentially represent the changes undergone in the ACC density structure south of Africa, thereby providing insight into the diabatic alterations that occurred over the observational period (Figure 6).

The rates of change evident in Figure 6 are in the same range as the adiabatic trends of Figure 5, yet the pattern is almost entirely in the opposite sense. Figure 6 shows a diabatic cooling (-0.7°C decade^{-1}) and salinification (-0.08 decade^{-1}) in the SAZ with the post-2005 GEM possessing lower temperatures and salinities than the earlier GEM. Positive differences representing a diabatic increase in heat (maximum 0.5°C decade^{-1}) and salt (maximum 0.1 decade) are visible south of the APF at around 1500 dbar corresponding to UCDW. Similar warming and salinification trends between the isopycnals 27.2–27.8 kg m^{-3} (AAIW and UCDW density range) were also noticed by *Meijers et al.* [2011a] in their assessment of circumpolar diabatic trends. A freshening can be seen in the top 200 dbar in the southern PFZ and the Antarctic Zone (AZ). The mean diabatic variability of the upper 2000 dbar of the ACC south of Africa is -0.044 ± 0.13°C decade^{-1} and -0.01 ± 0.017 decade^{-1} for T and S, respectively.

5.2. Combining Adiabatic and Diabatic Trends in an AD-AGEM

The time evolving AGEM T(x,y,p,t) and S(x,y,p,t) fields essentially only represent adiabatic alterations within the water column of the southeast Atlantic as the AGEM proxy technique horizontally rearranges the position of vertical T and S profiles in response to a change in the surface dynamic height. The AGEM does not modify the vertical structure of these profiles, and thus is unable to resolve property changes due to diabatic heat and salt fluxes at various depths. In this section, we investigate the changes occurring in the region from 1992 to 2012 by combining the adiabatic and diabatic components of change in an Adiabatic-

Diabatic AGEM (AD-AGEM). This is accomplished by following the technique explained in *Meijers et al.* [2011b], where the diabatic differences at each grid point (p,φ) are converted into trends per week, and are incrementally added to the original GEM fields as a function of time. The fields are projected back into η(x,y) space and the result is 20 years of AD-AGEM time evolving T(x,y,p,t) and S(x,y,p,t) sections that represent both the diabatic and adiabatic alterations of the ACC density field south of Africa.

The heat and salt contents of the ACC in this region can now be calculated from the resultant AD-AGEM fields. These values are integrated over the whole domain from the STF to the southern-most extent of altimetry data (this position varies depending on the extent of sea ice). The heat content (HC) and salt content (SC) of the upper 2000 dbar south of Africa are presented in Figure 7 and were calculated using the following equations:

$$HC = \int\int_{2000\ \mathrm{dbar}}^{5\ \mathrm{dbar}} pC_p\mathrm{T}\ \delta z \delta y$$

$$SC = \int\int_{2000\ \mathrm{dbar}}^{5\ \mathrm{dbar}} p0.001\ \mathrm{S}\ \delta z \delta y$$

where ρ is the density of seawater (1027 kg m^{-3}), Cp is the heat capacity of seawater at a constant pressure (4000 J kg^{-1} K^{-1}), z the depth range (5–2000 dbar) of the AGEM fields, y is the meridional extent of the ACC, T is the temperature (°C), and S is the salinity.

The HC and SC of the AD-AGEM fields are compared with the original AGEM fields in Figures 7a and 7c. The original AGEM estimates of both HC and SC of the upper 2000 dbar of the African sector of the ACC are greater than the AD-AGEM estimates, and the difference between the two increases with time. Inclusion of the diabatic trends into the time evolving AGEM fields appears to have partially lowered the HC (Figure 7a), and caused a significant decrease in the SC (Figure 7c). This signifies that although the southward displacement of the ACC fronts is driving an apparent adiabatic salinification within the ACC domain, the diabatic input of freshwater overrides this effect resulting in a net decrease in SC. There are both freshening and salinification trends in the adiabatic component that will partially offset one another, unlike the adiabatic T trends, which are positive throughout the section (Figure 5).

There is a clear increase in the overall HC of the ACC with time, as shown by the increasing values in Figure 2a and the prevalence of positive anomalies after 2007 in Figure 7b. The positive anomalies that were previously dominant in the SAZ (Figure 4a), now appear sizeably reduced due to diabatic cooling effects (∼−0.7°C $decade^{-1}$; Figure 6a) in this region. The opposite is true for the region south of the SAF where diabatic warming trends (∼0.6°C $decade^{-1}$ in the AZ; Figure 6a) have amplified the increase in mean temperature of the upper 2000 dbar due to the shift in fronts resulting in a coherent uniform distribution of positive T anomalies post-2005. Similar spatial separation of trends was noticed by *Gille* [2008] who described from summertime averages of the upper 1000 m a cooling north of the SAF and a warming to the south. The decrease in salt content is strongest in the SAZ, seen by the large negative anomalies in Figure 7d. The SC variations appear to be clearly divided by frontal zone, with strong freshening north of the SAF post-2002, no clear trend in anomalies within the PFZ, and an increase in positive T anomalies post-2007 in the region between the APF and the southern boundary of the ACC. Results from the AGEM including the diabatic components of change expose a small net freshening of the ACC within the African choke point (Figure 7c). Examination of the absolute property changes over time renders mean trends for the top 2000 dbar for the ACC south of Africa of 0.12 ± 0.087°C $decade^{-1}$ and −0.0039 ± 0.0017 $decade^{-1}$. The standard deviations of these estimates are large due to the highly variable nature of the longer-term variability with both depth and latitude, as can be seen in Figure 8, showing the T and S trends of the AD-AGEM fields significant at 95% confidence.

5.2.1. AAIW Evolution

It is important to obtain a better understanding of the thermohaline variability of AAIW, as it is widely thought to have a critical influence on ocean circulation and climate regulation. This water mass facilitates important transports of heat, freshwater, and biogeochemical tracers, both vertically from the surface to the interior ocean, and meridionally from the Southern Ocean to the tropics [*Sloyan and Rintoul*, 2001; *Pahnke et al.*, 2008]. After AAIW is formed, it subducts below the seasonal thermocline and is no longer in direct contact with the atmosphere, thereby retaining its properties set at formation [*Rimaud et al.*, 2012]. AAIW

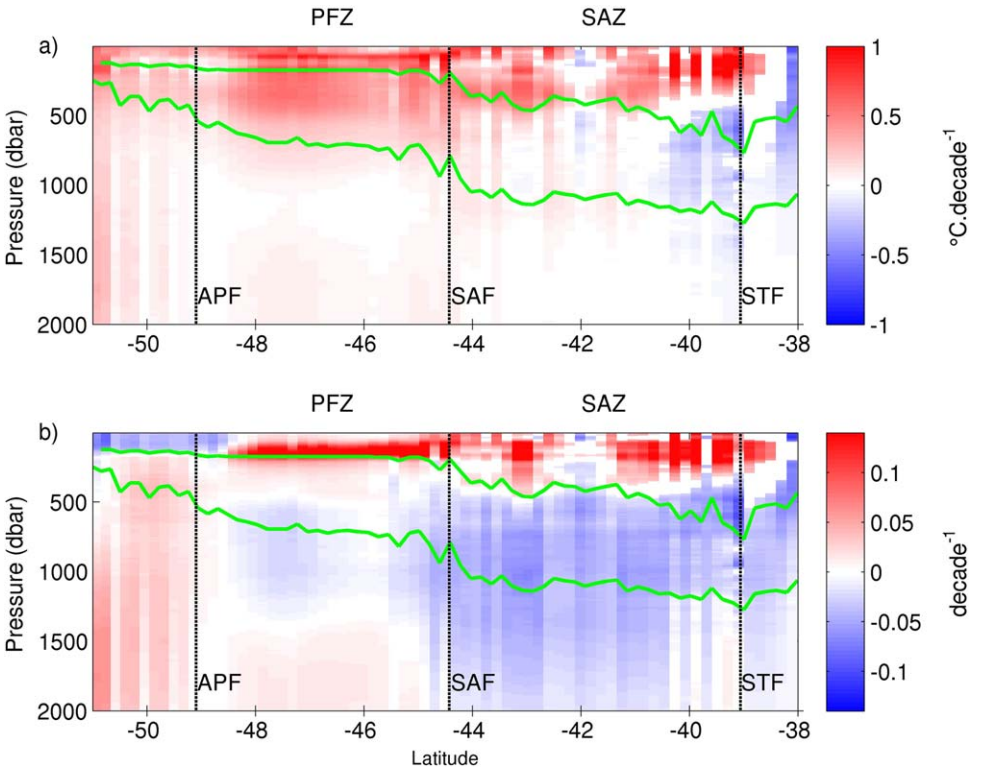

Figure 8. Mean AD-AGEM trends in (a) temperature (°C decade^{-1}) and (b) salinity (decade^{-1}) from 1992 to 2012. Only those significant at over 95% confidence have been shaded. The mean upper and lower limits of the AAIW layer are overlaid in green using the 27.0 and 27.4 kg m^{-3} density contours, respectively.

has its properties set west of Drake Passage, and undergoes further mixing in the Scotia Sea and Brazil/Malvinas confluence [*Talley*, 1996; *Naveira Garabato et al*., 2009]. We examine this water mass immediately downstream of its formation and modification region, at a point where its properties are relatively stable, and thus is an ideal place to examine longer-term trends due to changes in heat and freshwater fluxes.

The exact isopycnal interval of the AAIW layer at the GH line was identified from Argo float data by *Rusciano et al*. [2012] as being 27.1–27.32 kg m^{-3}. In order to account for the different varieties of AAIW that can be found south of Africa, we expand this range slightly to capture them all, and so the boundaries of AAIW used in this study are 27.0–27.4 kg m^{-3}. AAIW was identified in the AD-AGEM fields and the property information belonging to this layer extracted. The water mass is consistently located above 2000 dbar and therefore within the vertical limits of the Argo-based and cruise-based AGEM and is located within a depth range of the AGEM where the RMS errors are small ($T < 0.025$°C; $S < 0.001$) relative to the surface. The mean vertical limits of the AAIW layer can be seen in Figure 8 overlaid on the mean trends in T and S (significant at 95% confidence) of the AD-AGEM fields over the 20 year time period. In order to obtain improved insight into the spatial and temporal changes that AAIW has undergone between 1992 and 2012, the region is split up into latitudinal zones delimited by the position of the ACC fronts (see time varying positions in Figure 7). As the AD-AGEM fields are limited to south of 38°S, the location of the STF is bounded in the north by this latitude. For further insight into the horizontal pathways and varieties of AAIW within the southeast Atlantic domain please refer to *Rimaud et al*. [2012].

The temporal evolution of the T and S properties of the AAIW layer within the Subantarctic Zone (SAZ) are shown in Figure 9. The water mass layer averages of T and S decrease from 1992 to 2012 (Figures 9a and 9b) with trends of -0.17°C decade^{-1} ($r = -0.76$) and -0.032 ($r = -0.84$) for T and S, respectively. This net change in the water mass is the sum of both the adiabatic and diabatic alterations. The mean adiabatic trends for the AAIW layer located in the SAZ are 0.058°C decade^{-1} ($r = 0.36$) and 0.0076 decade^{-1} ($r = 0.35$) significant at 95% confidence for T and S, respectively. These trends can be seen in Figure 5, where a clear

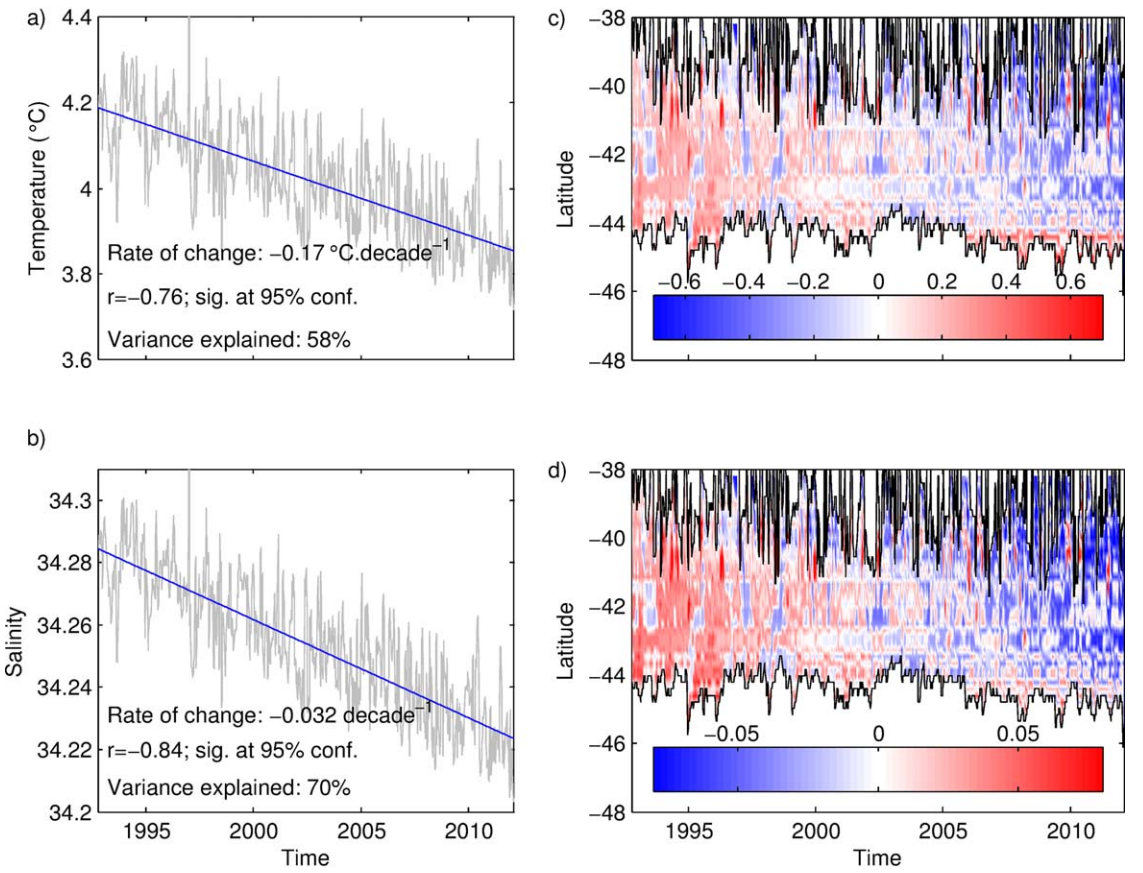

Figure 9. Mean (a) temperature and (b) salinity of AAIW within the SAZ. Hovmöller showing averaged anomalies in (c) temperature and (d) salinity of the AAIW water mass layer for the SAZ.

adiabatic warming is evident along with a sizeable increase in S within this water mass layer, changes typical of a southward shift in the fronts. The mean diabatic differences (Figure 6) of AAIW in the SAZ were found to be -0.23 ± 0.11°C decade^{-1} and -0.04 ± 0.015 decade^{-1}, indicating a cooling and freshening due to water mass fluxes. The standard deviations of the reported trends are large due to the broad distribution in values of the anomalies in this zone with both depth (Figure 8) and latitude (Figures 9c and 9d). The overall cooling and freshening of the SAZ can also been seen in the Hovmöller plots where there is a clear shift from positive to negative anomalies in 2002 (Figures 9c and 9d).

The thermohaline variability of AAIW for the Polar Frontal Zone (PFZ; Figure 10) displays a positive trend in both T and S over the past two decades. The property trends from the AD-AGEM fields from 1992 to 2012 are 0.31°C decade^{-1} (r = 0.83) and 0.014 decade^{-1} (r = 0.77). Pre-2005 there is very little change in AAIW properties with changes of 0.1°C decade^{-1} (r = 0.043) and 0.0026 decade^{-1} (r = 0.2) for T and S, respectively. Between 2005 and 2012, the rate of change increases with average trends of T and S of 0.54°C decade^{-1} (r = 7) and 0.027 decade^{-1} (r = 0.67). For clarity, we have presented the trends over the entire time period in Figures 10a and 10b, where the gradient of change for mean T of AAIW located in the PFZ is almost double that of the negative T change found in the SAZ. Figures 10c and 10d indicate a fairly even distribution of anomalies with latitude and a strong increase in positive values post-2006. The mean adiabatic trends for the AAIW layer located in the PFZ are 0.062°C decade^{-1} (r = 0.38) and 0.0037 decade^{-1} (r = 0.37) for T and S, respectively. The diabatic differences from hydrography alone are comparatively smaller with mean T trends of 0.25 ± 0.082°C decade^{-1} and S trend of 0.01 ± 0.011 decade^{-1} for AAIW located in this zone. Again, the standard deviations of the mean trends are large due to the presence of both positive and negative trends within the intermediate water mass layer of the PFZ (see Figures 5 and 6 between isopycnals 27.0–27.4 kg m^{-3}).

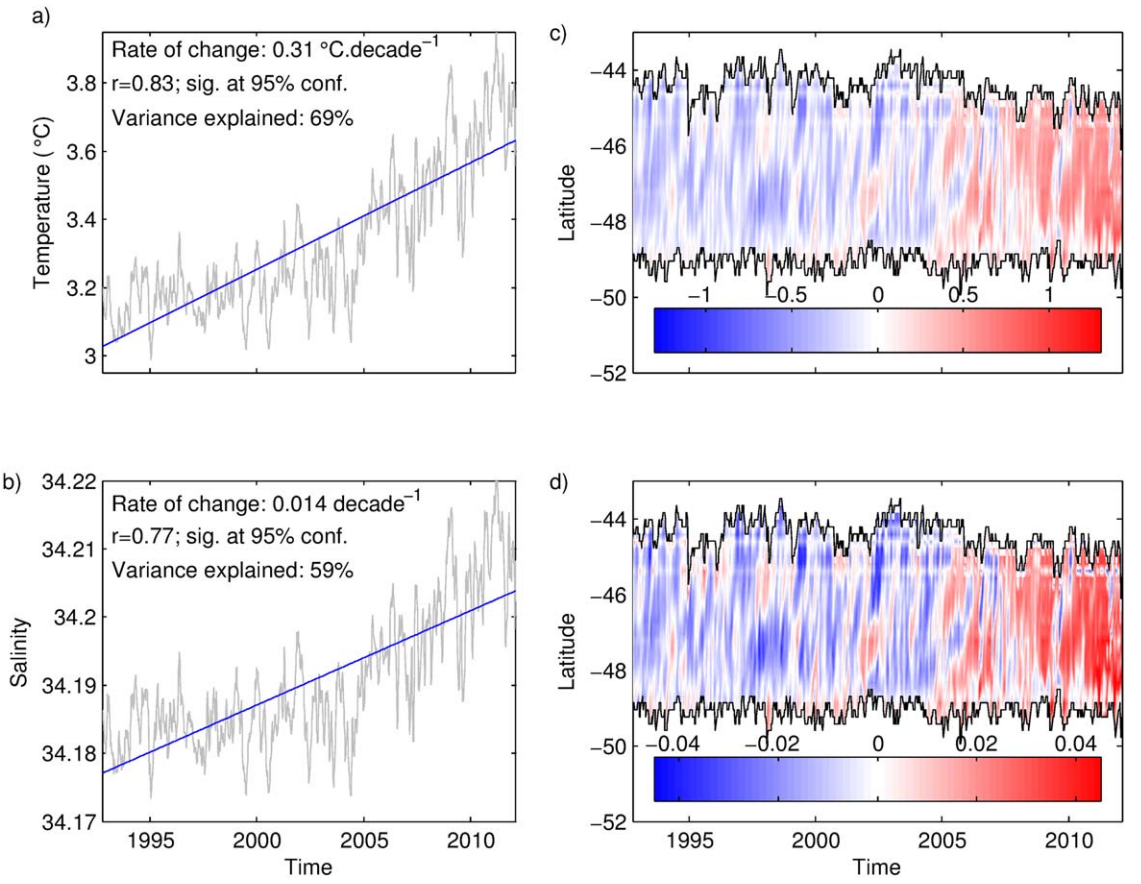

Figure 10. Mean (a) temperature and (b) salinity of AAIW within the PFZ. Hovmöller showing averaged anomalies in (c) temperature and (d) salinity of the AAIW water mass layer for the PFZ.

Gille [2002] showed using Lagrangian floats recording middepth temperatures in the Southern Ocean that temperatures in the intermediate layer (700–1100 m) have risen by 0.008°C yr^{-1} between the 1950s and the 1980s. The trends reported by *Gille* [2002] can largely be considered adiabatic as they are measured in a fixed depth/latitude range. The overall positive adiabatic alterations reported here for AAIW in both the SAZ and PFZ are in line with the trends reported by *Gille* [2002]. On the other hand, in a study using circumpolar Argo and CTD observations from the early 1960s, *Böning et al.* [2008] reported widespread cooling (-0.012 ± 0.005°C yr^{-1}) and freshening (-0.045 ± 0.02 yr^{-1}) north of the APF in the AAIW density class (27.1–27.2 kg m^{-3}), and warming and salinification trends in UCDW on the poleward flank of the ACC. These trends are closer to diabatic alterations by virtue of observing changes along a density surface. The diabatic trends in AAIW reported in this study indicate a cooling and freshening in the SAZ and a warming and salinification in the PFZ, thereby largely agreeing with the findings of *Böning et al.* [2008].

6. Discussion

6.1. Thermohaline Changes Within the ACC South of Africa

The contributors driving the long-term variations within the Atlantic sector of the Southern Ocean are complex to ascertain due to the multitude of factors influencing the ocean properties within the region. The southward movement of the ACC fronts [*Meijers et al.*, 2011b; *Fyfe and Saenko*, 2006; *Graham et al.*, 2012], increased Agulhas leakage [*Biastoch et al.*, 2009; *Durgadoo et al.*, 2013], changes in precipitation [*Durack et al.*, 2012], upstream processes [*Swart and Speich*, 2010], and sea ice melt [*Hall and Visbeck*, 2002; *Sen Gupta and England*, 2006] all have influential roles in determining the thermohaline properties in the southeast Atlantic. Identifying the contribution of each of these processes and the associated feedback and response mechanisms remains complex. Nevertheless, some hypotheses providing explanations for the observed changes are proposed.

In a recent study relevant to the ACC south of Africa, *Domingues et al*. [2014] showed that the ACC system is strongly linked to atmospheric forcing. It was found that upper ocean temperature variability is largely tied to wind forcing, with meridional changes in wind stress, linked to the Southern Annular Mode (SAM), driving changes in SAF and APF transports via Ekman dynamics. Latitudinal shifts in the Southern Hemisphere westerly winds may therefore play a significant role in generating observed adiabatic T and S changes. A tendency toward an increasing SAM in recent decades was observed by *Sallée et al*. [2010], implying a poleward shift and intensification of the westerlies [*Hall and Visbeck*, 2002; *Thompson and Solomon*, 2002; *Morrow et al*., 2008], and thus a southward shift in the fronts. The results pertaining to adiabatic fluctuations (Figures 4 and 5) exhibit similar spatial distribution of trends to those reported in other studies: *Morrow et al*. [2008] noticed a significant warming in the SAZ of $\sim$0.19°C yr^{-1} between two mean summertime sections of the ACC, and proposed it was due to the southward displacement of the fronts. As the AGEM measures the adiabatic shifts due to horizontal displacements of the water masses, the results displayed here can be directly compared with those *Morrow et al*. [2008] attributed due to frontal shifts. The reported 0.19°C yr^{-1} [*Morrow et al*., 2008] is almost double the maximum trend in the anomalies evident in Figure 5 of 0.12°C yr^{-1} (1.2°C decade^{-1}). The adiabatic salinity changes showing overall positive S anomalies equatorward of the SAF and freshening poleward (Figures 4 and 5) are congruent, for example, with those of *Boyer et al*. [2005], where positive S trends over the past 50 years were described in the subtropics and negative trends south of this. The dominant signal presented by *Meijers et al*. [2011b] is also in agreement with the results presented in Figure 5, namely significant warming and salinification in the upper 500 dbar. The theoretical explanation of these adiabatic alterations is that a southward displacement of the ACC would allow for the advection of warmer and saltier tropical waters into northern sector of the ACC (mainly the SAZ), thereby explaining the positive anomalies in the upper 1000 dbar seen in this region. Poleward of the SAZ, the variability is dominated by frontal meandering, largely due to the conservation of potential vorticity and baroclinic instability of the mean flow in response to the disturbance caused by local topography. The adiabatic freshening of the lower portion of the AAIW layer and UCDW observed in Figure 5b is likely caused by the southward shift of the low S tongue of AAIW, as would be the case with a southward movement of the ACC fronts.

The diabatic pattern of change presented in Figure 6 is complex to explain; however, some suggestions are presented here based on spatial agreements with the expected water mass alterations due to air-sea fluxes in response to climate change [*Banks and Bindoff*, 2003; *Aoki et al*., 2005]. *Durack and Wijffels* [2010] reported an increase in intensity of the global water cycle over the past 50 years, with *Durack et al*. [2012] later quantifying this change to report a 4% intensification in the cycle from 1950 to 2000. This implies elevated salt content in evaporation dominated regions (midlatitudes) and freshening in precipitation dominated regions (high latitudes). The prevalence of negative diabatic salt anomalies near the surface and in recently ventilated water masses south of the Polar Front (Figure 6) supports this hypothesis of increased precipitation in the high latitudes. The cause of the diabatic subsurface salinification throughout the ACC south of the SAF is unclear (Figure 6), however the freshening north of the SAF throughout the SAZ may be explained by the positive SAM. During a positive SAM, more warm moist air is able to shift further south with the poleward displacement of the atmospheric systems, thereby allowing for a freshening of the surface layers [*Hall and Visbeck*, 2002; *Morrow et al*., 2008; *Sallée et al*., 2010]. In addition, Subtropical air masses overlying polar water masses would drive increased heat flux from the atmosphere to the ocean, resulting in a diabatic warming of the upper ocean as is seen above 200 dbar south of the SAF (Figure 6).

Recent studies have shown that there has been a significant warming of the world's oceans [*Roemmich et al*., 2015]. *Levitus et al*. [2005] suggested from observations that over the past 40 years, approximately 84% of the total heating of the Earth's system has gone into the oceans. Two subsequent studies using the independent climate models Parallel Climate Model (PCM) and the Hadley Centre Coupled Model (HadCM3) concluded that results leave little doubt that a large portion of the signal is human induced and that the observed and model simulated anthropogenic warming are in agreement [*Barnett et al*., 2005; *Pierce et al*., 2006]. *Roemmich et al*. [2015] showed that from 2002 to 2013 ocean heat gain over the upper 2000 m of the world ocean continued at a rate of 0.4–0.6 W m^{-2}, with a broad intermediate depth maximum in heat gain between 700 and 1400 m. The model study of *Sallée et al*. [2010] further supports this, with the most consistent change under increased radiative forcing simulated across all models and water masses being a warming throughout the water-column. This warming is predicted to be largest in mode and intermediate layers, where a freshening is also reported to occur [*Sallée et al*., 2010]. It is thought that the Southern Ocean

is warming at a rate faster than the global average, and that this warming is largely localized to the ACC [*Gille*, 2002, 2008]. Estimates of ocean warming may be underestimated due to the conservative estimates in data sparse regions, such as the Southern Ocean where, until the recent introduction of Argo floats, the ability to detect upper ocean heat gain has been limited [*Durack et al*., 2012; *Roemmich et al*., 2015]. The results reported here are in line with observations and predictions from coupled numerical models (Figure 8). The net increase in HC in the sector of the ACC south of Africa (Figure 7a) is consistent with predictions of the oceanic response to climate change [*Bindoff and McDougall*, 1994; *Banks and Bindoff* 2003; *Aoki et al*., 2005; *Mayewski et al*., 2009; *Sallée et al*., 2010].

6.2. The Evolution of AAIW

Previous studies relying on observations alone have reported an overall warming and freshening of the ACC, with largest changes located in mode and intermediate layers [*Boyer et al*., 2005; *Gille*, 2008; *Böning et al*., 2008]. However, there have been some contradicting reports regarding the circumpolar alteration of the AAIW layer specifically, with *Arbic and Owens* [2001] reporting a climatic warming, and *Oke and England* [2004] finding a cooling along with an increase in formation rate. A study based on observations in the Drake Passage from 1969 to 2005 by *Naveira Garabato et al*. [2009] reported that ENSO dominates the forcing of inter-annual variations in AAIW properties resulting in a circumpolar warming and freshening of AAIW over the last five decades. The alteration of AAIW within the two frontal zones presented here exhibit entirely opposing net trends, thereby explaining a possible source of some of the contradicting conclusions of previous research. Even though the adiabatic changes throughout the ACC shown in Figure 5 posses positive average trends, the large negative diabatic changes in the SAZ (Figure 6) drive an overall decrease in heat and salt of the water mass in this area, compared to the positive diabatic changes in the PFZ that enforce the positive adiabatic trends resulting in an increase in T and S of AAIW in this zone. The warming trends of the PFZ could possibly be driven by increased heat flux due to the southward penetration of warmer air masses related to both the positive SAM and westerly wind shift. This air temperature-driven warming would only apply to shallow waters however, and thus a possible contribution to the subsurface diabatic salinification could be an increase in the upwelling of Circumpolar Deep Water (CDW). The results presented here highlight the importance of local investigations and separation of the temporal trends into adiabatic and diabatic components.

The differing thermohaline trends in AAIW between the SAZ and PFZ indicate that the water mass does not undergo high levels of meridional along-isopcynal mixing in Southern Ocean near the GoodHope line. It is hypothesized therefore that in this area, there is limited communication between AAIW residing within the same density class in the PFZ and the deep layers north of the SAF. This, in turn, implies that it is changes in the formation region of AAIW and modification along its path downstream that are more important in determining intermediate water variability than changes due to lateral mixing in the area. This hypothesis requires robust testing in future studies that take a closer look at the evolution of AAIW as it travels from its formation region to the subtopics.

An investigation into the temporal evolution of AAIW in the southeast Atlantic Ocean is highly relevant as the climatic equilibrium of the Atlantic depends on the preconditioning of waters in the southernmost sector [*Broecker*, 1991; *Marchesiello et al*., 1998]. The African choke point is where ACC transport and properties are thought to be the most variable [*Swart et al*., 2008], which has important implications for AAIW evolution in this region as instabilities in the ACC are thought to have a significant impact in the properties of AAIW [*Piola and Georgi*, 1982]. The sizeable magnitude of T trends, -0.17°C decade^{-1} ($r = -0.76$) in the SAZ and 0.31°C decade^{-1} ($r = 0.83$) PFZ, and the opposing trends within the same density class between frontal regions, together indicate that complex changes are occurring within the AAIW water mass in the ACC south of Africa.

7. Conclusion

The Southern Ocean is thought to be warming at a rate greater than the global ocean; however, due to limited observations, the specific regional variability of change is poorly understood [*Gille*, 2002, 2008; *Mayewski et al*., 2009]. The AD-AGEM presented here provides a robust technique to investigate the thermohaline evolution of the ACC in the southeast Atlantic. The AGEM projection combined with differences in temporal GEMs enable the separation of the observed changes into their adiabatic and diabatic components. These trends show an adiabatic overall warming of the upper 2000 dbar of the ACC south of Africa with strongest

changes located in the surface waters of the SAZ. Adiabatic salinification evident in the upper 1000 dbar in the SAZ is contrasted with significant freshening at intermediate depths of the PFZ. Diabatic trends in the SAZ produced thermohaline changes entirely opposed to the trends due to a shift in fronts, dominating the net changes in this area. Positive diabatic trends in the PFZ, on the other hand, act to amplify the adiabatic trends in this zone thereby resulting in net warming and salinification signals. The mean property changes for the top 2000 dbar of the ACC south of Africa from the AD-AGEM (adiabatic + diabatic changes AGEM) indicate a warming of 0.12 ± 0.087°C decade^{-1} and a minor freshening of -0.0039 ± 0.0017 decade^{-1}. Both the unmodified GEM and AD-AGEM possess trends indicating an increase in mean heat content of the upper 2000 dbar of the ACC in the region.

Mean trends of AAIW in the SAZ were comprised of positive adiabatic trends and negative diabatic trends, with the latter having a dominant effect producing results that show a cooling and freshening of intermediate water in the northern domain of the ACC south of Africa. Overall, positive adiabatic and diabatic trends in the PFZ create a cumulative warming and salinification effect to the south of the SAF. These apparent differing trends imply that either the water masses of the same density class in these zones undergo very little mixing along density surfaces, or that there is a high degree of spatial variability in the surface forcing and that the time scales over which this study is conducted are not long enough to capture the mixing effect of a warming and salinification in the south, on the water mass layer to the north. Despite the limitations that exist when using the GEM proxy technique, the resultant AD-AGEM weekly updated thermohaline sections of the Southern Ocean south of Africa have proven their usefulness in investigating the thermohaline evolution of water masses in this critical choke point of the ACC over the past 20 years.

Acknowledgments

The authors would like to acknowledge the financial support necessary to carry out this research provided by the South African National Research Fund (NRF), the South African National Antarctic Programme (SANAP; S. Swart SANAP grant SNA14071475720), the South Atlantic Meridional Overturning Circulation (SAMOC) group, and the Council for Scientific and Industrial Research (CSIR). This study would not have been possible without the data collected by the hydrographic cruises conducted under the auspices of the Alfred Wegener Institute aboard the RV Polarstern, the Shirshov Institute of Oceanology aboard the RV Akademik Sergey Vavilov, and the BONUS-GoodHope campaign aboard the RV Marion Dufresne, and the float data collected thanks to the Argo profiling float network and collected at the Coriolis Data Center. The CTD data can be obtained by contacting Associate Professor Isabelle Ansorge (isabelle.ansorge@uct.ac.za) or Professor Sabrina Speich (speech@lmd.ens.fr) and the Argo data can be found at the following web address: http://www.argodatamgt.org/Documentation/Access-via-ftp-on-GDAC, or ftp address: ftp://ftp.ifremer.fr/ifremer/argo. The satellite measurements are available from AVISO at: http://www.aviso.altimetry.fr/en/data/products/auxiliary-products/mdt.html. The authors would like to extend our thanks to the reviewers for their valuable contributions and suggestions that helped improve this paper.

References

Aoki, S., N. L. Bindoff, and J. A. Church (2005), Interdecadal water mass changes in the Southern Ocean between 30°E and 160°E, *Geophys. Res. Lett.*, *32*, L07607, doi:10.1029/2004GL022220.

Arbic, B. K., and W. B. Owens (2001), Climatic warming of Atlantic intermediate waters*, *J. Clim.*, *14*(20), 4091–4108.

Banks, H. T., and N. L. Bindoff (2003), Comparison of observed temperature and salinity changes in the Indo-Pacific with results from the coupled climate model HadCM3: Processes and mechanisms*, *J. Clim.*, *16*(1), 156–166.

Banks, H. T., R. A. Wood, J. M. Gregory, T. C. Johns, and G. S. Jones (2000), Are observed decadal changes in intermediate water masses a signature of anthropogenic climate change?, *Geophys. Res. Lett.*, *27*(18), 2961–2964.

Barnett, T. P., D. W. Pierce, K. M. AchutaRao, P. J. Gleckler, B. D. Santer, J. M. Gregory, and W. M. Washington (2005), Penetration of human-induced warming into the world's oceans, *Science.*, *309*(5732), 284–287.

Biastoch, A., C. W. Böning, F. U. Schwarzkopf, and J. Lutjeharms (2009), Increase in Agulhas leakage due to poleward shift of Southern Hemisphere westerlies, *Nature*, *462*(7272), 495–498.

Bindoff, N. L., and T. J. McDougall (1994), Diagnosing climate change and ocean ventilation using hydrographic data, *J. Phys. Oceanogr.*, *24*(6), 1137–1152.

Boebel, O., J. Lutjeharms, C. Schmid, W. Zenk, T. Rossby, and C. Barron (2003), The Cape Cauldron: A regime of turbulent inter-ocean exchange, *Deep Sea Res., Part II*, *50*(1), 57–86.

Böning, C. W., A. Dispert, M. Visbeck, S. Rintoul, and F. Schwarzkopf (2008), The response of the Antarctic Circumpolar Current to recent climate change, *Nat. Geosci.*, *1*(12), 864–869.

Boyer, T. P., S. Levitus, J. Antonov, R. Locarnini, and H. Garcia (2005), Linear trends in salinity for the World Ocean, 1955–1998, *Geophys. Res. Lett.*, *32*, L01604, doi:10.1029/2004GL021791.

Broecker, W. S. (1991), The great ocean conveyor, *Oceanography*, *4*(2), 79–89.

Dencausse, G., M. Arhan, and S. Speich (2010), Routes of Agulhas rings in the southeastern Cape Basin, *Deep Sea Res., Part I*, *57*(11), 1406–1421.

Domingues, R., G. Goni, S. Swart, and S. Dong (2014), Wind forced variability of the Antarctic Circumpolar Current south of Africa between 1993 and 2010, *J. Geophys. Res. Oceans*, *119*, 1123–1145, doi:10.1002/2013JC008908.

Ducet, N., P. Le Traon, and G. Reverdin (2000), Global high-resolution mapping of ocean circulation from TOPEX/Poseidon and ERS-1 and-2, *J. Geophys. Res.*, *105*(C8), 19,477–19,498.

Durack, P. J., and S. E. Wijffels (2010), Fifty-year trends in global ocean salinities and their relationship to broad-scale warming, *J. Clim.*, *23*(16), 4342–4362.

Durack, P. J., S. E. Wijffels, and R. J. Matear (2012), Ocean salinities reveal strong global water cycle intensification during 1950 to 2000, *Science*, *336*(6080), 455–458, doi:10.1126/science.1212222.

Durgadoo, J. V., B. R. Loveday, C. J. Reason, P. Penven, and A. Biastoch (2013), Agulhas leakage predominantly responds to the Southern Hemisphere westerlies, *J. Phys. Oceanogr.*, *43*(10), 2113–2131.

Firing, Y. L., T. K. Chereskin, and M. R. Mazloff (2011), Vertical structure and transport of the Antarctic Circumpolar Current in Drake Passage from direct velocity observations, *J. Geophys. Res.*, *116*, C08015, doi:10.1029/2011JC006999.

Fu, L. (1981), The general circulation and meridional heat transport of the subtropical South Atlantic determined by inverse methods, *J. Phys. Oceanogr.*, *11*(9), 1171–1193.

Fyfe, J. C., and O. A. Saenko (2006), Simulated changes in the extratropical Southern Hemisphere winds and currents, *Geophys. Res. Lett.*, *33*, L06701, doi:10.1029/2005GL025332.

Garzoli, S. L., and R. Matano (2011), The South Atlantic and the Atlantic meridional overturning circulation, *Deep Sea Res., Part II*, *58*(17), 1837–1847.

Gille, S. T. (2002), Warming of the Southern Ocean since the 1950s, *Science*, *295*(5558), 1275–1277, doi:10.1126/science.1065863.

Gille, S. T. (2008), Decadal-scale temperature trends in the Southern Hemisphere ocean, *J. Clim.*, *21*(18), 4749–4765.
Gladyshev, S., M. Arhan, A. Sokov, and S. Speich (2008), A hydrographic section from South Africa to the southern limit of the Antarctic Circumpolar Current at the Greenwich meridian, *Deep Sea Res., Part I*, *55*(10), 1284–1303.
Gould, J., D. Roemmich, S. Wijffels, H. Freeland, M. Ignaszewsky, X. Jianping, S. Pouliquen, Y. Desaubies, U. Send, and K. Radhakrishnan (2004), Argo profiling floats bring new era of in situ ocean observations, *EOS Trans. AGU*, *85*(19), 185–191.
Graham, R. M., A. M Boer, K. J. Heywood, M. R. Chapman, and D. P. Stevens (2012), Southern Ocean fronts: Controlled by wind or topography?, *J. Geophys. Res.*, *117*, C08018, doi:10.1029/2012JC007887.
Hall, A., and M. Visbeck (2002), Synchronous variability in the Southern Hemisphere atmosphere, sea ice, and ocean resulting from the Annular Mode*, *J. Clim.*, *15*(21), 3043–3057.
Holfort, J., and G. Siedler (2001), The meridional oceanic transports of heat and nutrients in the South Atlantic, *J. Phys. Oceanogr.*, *31*(1), 5–29.
Jacobs, S. (2006), Observations of change in the Southern Ocean, *Philos. Trans. R. Soc. A*, *364*(1844), 1657–1681, doi:10.1098/rsta.2006.1794.
Killworth, P. D. (1992), An equivalent-barotropic mode in the Fine Resolution Antarctic Model, *J. Phys. Oceanogr.*, *22*(11), 1379–1387.
Killworth, P. D., and C. W. Hughes (2002), The Antarctic Circumpolar Current as a free equivalent-barotropic jet, *J. Mar. Res.*, *60*(1), 19–45.
Lemke, P. (1992), *WHP cruise summary information*, technical report, Alfred Wegener Inst. fuer Polarforsch. und Meeresforsch., Bremerhaven, Germany.
Le Traon, P., and F. Ogor (1998), ERS-1/2 orbit improvement using TOPEX/POSEIDON: The 2 cm challenge, *J. Geophys. Res.*, *103*(C4), 8045–8057.
Le Traon, P., F. Nadal, and N. Ducet (1998), An improved mapping method of multisatellite altimeter data, *J. Atmos. Oceanic Technol.*, *15*(2), 522–534.
Locarnini, R., et al. (2013), *World Ocean Atlas 2013*, vol. 1, *Temperature*, *NOAA Atlas NESDIS 73*, 40 pp.
Lutjeharms, J. (1996), The exchange of water between the South Indian and South Atlantic Oceans, in *The South Atlantic*, pp. 125–162, Springer, Berlin Heidelberg.
Marchesiello, P., B. Barnier, and A. P. de Miranda (1998), A sigma-coordinate primitive equation model for studying the circulation in the South Atlantic Part II: Meridional transports and seasonal variability, *Deep Sea Res., Part I*, *45*(4), 573–608.
Marshall, J., and K. Speer (2012), Closure of the meridional overturning circulation through Southern Ocean upwelling, *Nat. Geosci.*, *5*(3), 171–180.
Mayewski, P. A., M. Meredith, C. Summerhayes, J. Turner, A. Worby, P. Barrett, G. Casassa, N. A. Bertler, T. Bracegirdle, and A. Naveira Garabato (2009), State of the Antarctic and Southern Ocean climate system, *Rev. Geophys.*, *47*, RG1003, doi:10.1029/2007RG000231.
Meijers, A., N. Bindoff, and S. Rintoul (2011a), Estimating the four-dimensional structure of the Southern Ocean using satellite altimetry, *J. Atmos. Oceanic Technol.*, *28*(4), 548–568.
Meijers, A., N. Bindoff, and S. Rintoul (2011b), Frontal movements and property fluxes: Contributions to heat and freshwater trends in the Southern Ocean, *J. Geophys. Res.*, *116*, C08024, doi:10.1029/2010JC006832.
Meinen, C. S., and D. R. Watts (2000), Vertical structure and transport on a transect across the North Atlantic Current near 42 N: Time series and mean, *J. Geophys. Res.*, *105*(C9), 21,869–21,891.
Meredith, M. P., and A. M. Hogg (2006), Circumpolar response of Southern Ocean eddy activity to a change in the Southern Annular Mode, *Geophys. Res. Lett.*, *33*, L16608, doi:10.1029/2006GL026499.
Morrow, R., G. Valladeau, and J. Sallee (2008), Observed subsurface signature of Southern Ocean sea level rise, *Prog. Oceanogr.*, *77*(4), 351–366.
Naveira Garabato, A. C., L. Jullion, D. P. Stevens, K. J. Heywood, and B. A. King (2009), Variability of Subantarctic mode water and Antarctic intermediate water in the Drake Passage during the late-twentieth and early-twenty-first centuries, *J. Clim.*, *22*(13), 3661–3688.
Oke, P. R., and M. H. England (2004), Oceanic response to changes in the latitude of the Southern Hemisphere subpolar westerly winds, *J. Clim.*, *17*(5), 1040–1054.
Pahnke, K., S. L. Goldstein, and S. R. Hemming (2008), Abrupt changes in Antarctic Intermediate Water circulation over the past 25,000 years, *Nat. Geosci.*, *1*(12), 870–874.
Pierce, D. W., T. P. Barnett, K. M. AchutaRao, P. J. Gleckler, J. M. Gregory, and W. M. Washington (2006), Anthropogenic warming of the oceans: Observations and model results, *J. Clim.*, *19*(10), 1873–1900.
Piola, A. R., and D. T. Georgi (1982), Circumpolar properties of Antarctic intermediate water and Subantarctic Mode Water, *Deep Sea Res., Part A*, *29*(6), 687–711.
Rimaud, J., S. Speich, B. Blanke, and N. Grima (2012), The exchange of Intermediate Water in the southeast Atlantic: Water mass transformations diagnosed from the Lagrangian analysis of a regional ocean model, *J. Geophys. Res.*, *117*, C08034, doi:10.1029/2012JC008059.
Rio, M. H., P. Schaeffer, G. Moreaux, J. M. Lemoine, and E. Bronner (2009), A new mean dynamic topography computed over the global ocean from GRACE data, altimetry and in-situ measurements, in Poster communication at OceanObs09 symposium, vol. 25.
Riser, S. C., et al. (2016), Fifteen years of ocean observations with the global Argo array, *Nat. Clim. Change*, *6*(2), 145–153.
Roemmich, D., J. Church, J. Gilson, D. Monselesan, P. Sutton, and S. Wijffels (2015), Unabated planetary warming and its ocean structure since 2006, *Nat. Clim. Change*, *5*, 240–245.
Roemmich, D. H., R. E. Davis, S. C. Riser, W. B. Owens, R. L. Molinari, S. L. Garzoli, and G. C. Johnson (2003), The Argo project: Global ocean observations for understanding and prediction of climate variability, Scripps Institution of Oceanography, La Jolla, Calif.
Roether, W., M. Samthein, T. J. Muller, W. Nellen, and D. Sahrhage (1990), Sudatlantik-zircumpolarstrom, reise nr. 11, 3 Oktober 1989–11 Marz 1990, meteor-ber. 90-2, technical report, Univ. of Hamburg, Hamburg, Germany.
Rusciano, E., S. Speich, and M. Ollitrault (2012), Interocean exchanges and the spreading of Antarctic Intermediate Water south of Africa, *J. Geophys. Res.*, *117*, C10010, doi:10.1029/2012JC008266.
Sallée, J., K. Speer, and S. Rintoul (2010), Zonally asymmetric response of the Southern Ocean mixed-layer depth to the Southern Annular Mode, *Nat. Geosci.*, *3*(4), 273–279.
Schmidtko, S., and G. C. Johnson (2012), Multidecadal warming and shoaling of Antarctic Intermediate Water, *J. Clim.*, *25*(1), 207–221.
Sen Gupta, A., and M. H. England (2006), Coupled ocean-atmosphere-ice response to variations in the Southern Annular Mode, *J. Clim.*, *19*(18), 4457–4486.
Sloyan, B. M., and S. R. Rintoul (2001), Circulation, renewal, and modification of Antarctic mode and intermediate water*, *J. Phys. Oceanogr.*, *31*(4), 1005–1030.
Sokolov, S., B. A. King, S. R. Rintoul, and R. L. Rojas (2004), Upper ocean temperature and the baroclinic transport stream function relationship in Drake Passage, *J. Geophys. Res.*, *109*, C05001, doi:10.1029/2003JC002010.
Sparrow, M., P. Chapman and J. Gould (2005), The World Ocean Circulation Experiment (WOCE) Hydrographic Atlas Series.

Speich, S., and M. Arhan (2007), GOODHOPE/Southern Ocean: A study and monitoring of the Indo-Atlantic connections, *Mercator Newsl.*, *27*, 29–41.
Speich, S., and G. Dehairs (2008), Cruise Report, MD 66 BONUSGOODHOPE, Internal Report, 246 pp.
Speich, S., J. Lutjeharms, P. Penven, and B. Blanke (2006), Role of bathymetry in Agulhas Current configuration and behaviour, *Geophys. Res. Lett.*, *33*, L23611, doi:10.1029/2006GL027157.
Sun, C., and D. R. Watts (2001), A circumpolar gravest empirical mode for the Southern Ocean hydrography, *J. Geophys. Res.*, *106*(C2), 2833–2855.
Sun, C., and D. R. Watts (2002), A view of ACC fronts in streamfunction space, *Deep Sea Res., Part I*, *49*(7), 1141–1164.
Swart, S., and S. Speich (2010), An altimetry-based gravest empirical mode south of Africa: 2. Dynamic nature of the Antarctic Circumpolar Current fronts, *J. Geophys. Res.*, *115*, C03003, doi:10.1029/2009JC005300.
Swart, S., S. Speich, I. J. Ansorge, G. J. Goni, S. Gladyshev, and J. R. Lutjeharms (2008), Transport and variability of the Antarctic Circumpolar Current south of Africa, *J. Geophys. Res.*, *113*, C09014, doi:10.1029/2007JC004223.
Swart, S., S. Speich, I. J. Ansorge, and J. R. Lutjeharms (2010), An altimetry-based gravest empirical mode south of Africa: 1. Development and validation, *J. Geophys. Res.*, *115*, C03002, doi:10.1029/2009JC005299.
Talley, L. (1996), Antarctic intermediate water in the South Atlantic, in *The South Atlantic*, pp. 219–238, Springer, Berlin Heidelberg.
Thomson, R. E., and W. J. Emery (2014), *Data Analysis Methods in Physical Oceanography*, Elsevier.
Thompson, D. W. J., and S. Solomon (2002), Interpretation of recent Southern Hemisphere climate change, *Science*, *296*, 895–899.
Vivier, F., K. A. Kelly, and M. Harismendy (2005), Causes of large-scale sea level variations in the Southern Ocean: Analyses of sea level and a barotropic model, *J. Geophys. Res.*, *110*, C09014, doi:10.1029/2004JC002773.
Watts, D. R., C. Sun, and S. Rintoul (2001), A two-dimensional gravest empirical mode determined from hydrographic observations in the Subantarctic Front, *J. Phys. Oceanogr.*, *31*(8), 2186–2209.
Whitworth, T., III, and R. Peterson (1985), Volume transport of the Antarctic Circumpolar Current from bottom pressure measurements, *J. Phys. Oceanogr.*, *15*(6), 810–816.
Zweng, M. M, et al. (2013), *World Ocean Atlas 2013, vol. 2, Salinity, NOAA Atlas NESDIS 74*, 39 pp.